

1 **Lack of detectable neoantigen depletion signals in the untreated**  
2 **cancer genome**

3

4 Jimmy Van den Eynden<sup>1,2,3\*</sup>, Alejandro Jiménez-Sánchez<sup>3,4</sup>, Martin L. Miller<sup>3</sup> and Erik  
5 Larsson<sup>1,3</sup>

6

7 <sup>1</sup>Department of Medical Biochemistry and Cell Biology, Institute of Biomedicine, The  
8 Sahlgrenska Academy, University of Gothenburg, Gothenburg, Sweden.

9 <sup>2</sup>Department of Human Structure and Repair, Anatomy and Embryology Unit, Ghent  
10 University, Ghent, Belgium.

11 <sup>3</sup>Cancer Research UK Cambridge Institute, University of Cambridge, Li Ka Shing Centre,  
12 Robinson Way, Cambridge, UK.

13 <sup>4</sup>Program for Computational and Systems Biology, Sloan Kettering Institute, Memorial Sloan  
14 Kettering Cancer Center, New York, NY, USA.

15 \*Email: [jimmy.vandeneeynden@ugent.be](mailto:jimmy.vandeneeynden@ugent.be)

16 **Somatic mutations can result in the formation of neoantigens, immunogenic peptides**  
17 **that are presented on the tumor cell surface via HLA molecules. These mutations are**  
18 **expected to be under negative selection pressure, but the extent of the resulting**  
19 **neoantigen depletion remains unclear. Based on HLA affinity predictions, we**  
20 **annotated the human genome for its translatability to HLA binding peptides and**  
21 **screened for reduced single nucleotide substitution rates in large genomic datasets**  
22 **from untreated cancers. Apparent neoantigen depletion signals became negligible**  
23 **when considering trinucleotide-based mutational signatures, either due to lack of**  
24 **power or efficient immune evasion mechanisms active early during tumor evolution.**

25 Cancer is caused by somatic mutations in driver genes. These genomic alterations result in  
26 a selective growth advantage and positive selection of the affected cells<sup>1</sup>. With the rise of  
27 next-generation sequencing technologies, increasing insights into the cancer genome have  
28 led to a comprehensive characterization of the frequencies and patterns of somatic  
29 mutations across different cancers<sup>2,3</sup>. For a tumor to evolve, it also needs to develop ways to  
30 avoid immune destruction, a process referred to as immunoediting and one of the more  
31 recent hallmarks of cancer<sup>4,5</sup>. Mouse studies have shown that T lymphocyte recognition of  
32 tumor-specific antigens is crucial for immunoediting to occur<sup>6</sup>. The accumulation of somatic  
33 mutations in the tumor genome results in the formation of neoantigens, small peptides  
34 presented on the cell surface that can stimulate cytotoxic (CD8+) T lymphocytes (CTLs). To  
35 attenuate these CTL responses, a cancer cell can upregulate ligands for checkpoint  
36 receptors<sup>7</sup>. Therapeutically blocking these checkpoint pathways has been shown effective in  
37 several cancers such as metastatic melanoma and non-small cell lung cancer<sup>7-9</sup>. However,  
38 responses to immune checkpoint blockade (ICB) therapy are still largely unpredictable, and  
39 it is not completely understood why some tumors do not respond or develop resistance to  
40 therapy.

41         Several genomic alterations (e.g. *CASP8* mutations, *B2M* mutations, *HLA* loss) have  
42 been discovered that can partially explain this ICB therapy unresponsiveness<sup>10-16</sup>.  
43 Furthermore, as stimulation of CTLs is critically dependent on the formation and presentation  
44 of neoantigens, it is not surprising that one of the main determinants of therapy  
45 responsiveness is mutation burden<sup>17-19</sup>. Indeed, the higher the mutation burden, the higher  
46 the number of potential neoantigens and hence ways to stimulate the immune system. On  
47 the other hand, negative (or purifying) selection is expected to act on neoantigen-forming  
48 mutations. This should result in a depletion of such mutations and escape from immune-  
49 induced cancer cell death. The presence of neoantigen depletion has been suggested in  
50 several cancers such as colorectal cancer, metastatic melanoma, esophageal, bladder,  
51 cervical and lung cancer<sup>10,13,20,21</sup>. As the main determinant of CTL immunogenicity is a  
52 peptide's capacity to bind to the cell's human leukocyte antigens (HLA) from the type I major

53 histocompatibility complex (MHC-I), the conclusions of these studies are mostly based on  
54 lower-than-expected numbers of non-synonymous somatic mutations in predicted HLA-  
55 binding peptides, using the number of synonymous mutations as a reference.

56 Somatic mutations are caused by different mutational processes that are active  
57 during tumor evolution. A widely used method for characterizing the properties of mutational  
58 processes are trinucleotide-based mutational signatures, which describe frequencies for all  
59 single nucleotide substitutions in all possible sequence contexts in terms of adjacent  
60 upstream and downstream nucleotides, resulting in a total of 96 substitution types<sup>3</sup>. This  
61 implies that the mutation probability at any genomic position is dependent on the immediate  
62 sequence context in combination with the active mutational processes. It has now been  
63 clearly demonstrated that mutational signatures need to be accounted for in any model  
64 aiming at finding signals of selection in cancer<sup>22-24</sup>. However, it is currently not clear whether  
65 and how mutational signatures and their sequence context preferences influence signals of  
66 neoantigen depletion.

67 Here we show that, when mutational signatures are considered, putative signals of  
68 neoantigen depletion become weak to absent in cancer genomics data from treatment-naïve  
69 tumor samples. Our results are in line with the overall weak signals of negative selection in  
70 cancer and challenge the idea that neoantigen depletion signals are detectable based on  
71 HLA affinity predictions in large-scale cancer mutation datasets.

## 72 **RESULTS**

### 73 **Annotation of HLA-binding regions in the human genome.**

74 Somatic mutations are expected to result in neoantigen formation when (i) the resulting  
75 peptides are presented via MHC-I and (ii) they are recognized by CTLs through specific T-  
76 cell receptor (TCR) binding, which only occurs when there is no immune tolerance, i.e. when  
77 presented peptides are new to the immune system. Given sufficient co-stimulatory signals,  
78 this will result in CTL-mediated killing of neoantigen-presenting cancer cells, enforcing a

79 negative selection pressure during tumor evolution (Fig. 1a). We hypothesized that this  
80 specific form of negative selection and hence neoantigen depletion should be detectable as  
81 reduced mutation rates in genomic regions that can be translated to HLA-binding peptides.  
82 Therefore, our first aim was to define these regions, thereby generating an HLA-binding  
83 genomic annotation.

84 HLA-binding affinities are determined by both the amino acid sequence and by  
85 patient-specific HLA genotypes, composed of a combination of two HLA-A, two HLA-B and  
86 two HLA-C alleles. We initially considered a single prototypical HLA genotype consisting of  
87 the two most common HLA-alleles (HLA-A01:01, HLA-A02:01 HLA-B07:02, HLA-B08:01,  
88 HLA-C07:01 and HLA-C07:02; Supplementary Fig. 1), enabling us to define a single HLA-  
89 binding genome annotation to use throughout the analyses. For these six HLA alleles, the  
90 affinities were predicted for all possible nonapeptides (9-mers) translated from the coding  
91 genome and were aggregated in a single affinity, a similar approach to what has been  
92 described recently<sup>25</sup> (see Methods and Supplementary Fig. 1). By considering a nonapeptide  
93 HLA-binding when the aggregated  $K_d$  was lower than 500 nM<sup>26</sup>, we found that the complete  
94 pool of HLA-binding nonapeptides mapped to 22.1% of the exome (Fig. 1b).

#### 95 **Apparent negative selection signals in HLA-binding regions.**

96 Having annotated the human exome for the HLA-binding properties of its translated peptides,  
97 we next aimed to search for signals of immune-induced negative selection in the cancer  
98 genome. All available synonymous and non-synonymous (i.e. missense) somatic mutation  
99 data were downloaded from The Cancer Genome Atlas (TCGA), encompassing 1,836,369  
100 mutations from 8,683 different samples and spanning 32 cancer types (Supplementary Table  
101 1). As only non-synonymous mutations in HLA-binding regions are expected to be under  
102 immunogenic selection pressure, we used the number of synonymous mutations as a  
103 background reference and determined the ratio between the observed numbers of non-  
104 synonymous and synonymous mutations (n/s) in HLA-binding as well as non-binding regions.  
105 We found that n/s was lower in HLA-binding regions on a pan-cancer level (n/s 2.23 in HLA-

106 binding vs. 2.58 in non-binding regions,  $P = 3.24 \times 10^{-298}$ , Fisher's exact test; Fig. 2a,b). To  
107 quantify the extent of this putative neoantigen depletion signal, we defined an HLA-binding  
108 mutation ratio (HBMR) as the ratio of n/s in HLA-binding to non-binding peptides. This way,  
109 negative immunogenic selection of somatic mutations is expected to result in HBMR values  
110 lower than 1 (or higher than 1 if these mutations have been influenced by positive selection).  
111 For the pan-cancer analysis this implied an HBMR of 0.87, suggesting the overall loss of 13%  
112 of non-synonymous mutations due to negative selection (Fig. 2a,b).

113 We next aimed to determine how these signals differed between cancer types  
114 focusing on the 19 cancer types with at least 10,000 mutations in the TCGA dataset. Given  
115 the observed mutation burdens, we estimate sufficient power (0.8 at  $P < 0.05$ ) to detect  
116 negative selection operating on between 2% (UCEC) and 13% (KIRP) of the predicted  
117 neoantigens (Supplementary Fig. 2). We observed HBMR values that were significantly  
118 below 1 for 12 out of 19 analyzed cancer types, including bladder cancer (BLCA, HBMR =  
119 0.66,  $P = 1.5 \times 10^{-127}$ ), metastatic melanoma (SKCM, HBMR = 0.69,  $P = 0$ ), cervical cancer  
120 (CESC, HBMR = 0.72,  $P = 1.3 \times 10^{-51}$ ), lung adenocarcinoma (LUAD, HBMR = 0.77,  $P = 2.3$   
121  $\times 10^{-60}$ ), head and neck cancer (HNSC, HBMR = 0.78,  $P = 6.6 \times 10^{-36}$ ) and squamous cell  
122 lung cancer (LUSC, HBMR = 0.80,  $P = 1.4 \times 10^{-34}$ ) (Fig. 2c and Supplementary Table 2).

### 123 **Reduced non-synonymous mutations in HLA-binding regions are not caused by** 124 **selection processes.**

125 To be able to determine whether and to what extent selection processes and hence  
126 neoantigen depletion are indeed responsible for the observed reduction in non-synonymous  
127 mutations in HLA-binding regions, we determined the expected mutation rates in the  
128 absence of any selection pressure. For every observed somatic mutation, we simulated one  
129 mutation by randomly sampling from all possible point mutations with the same trinucleotide  
130 substitution type (e.g. TCC>TTC), resulting in a simulated mutation dataset with a similar  
131 size as the observed data. As expected, all signals of positive selection in driver genes  
132 disappeared in the simulated mutation data (Supplementary Fig. 3). Using this simulated

133 mutation database, we recalculated the mutation rates and HBMR values. Strikingly, a  
134 strong signal of apparent negative selection and hence neoantigen depletion, similar to the  
135 real mutation data, was still present (HBMR = 0.83,  $P = 0$ ; Fig. 2b). This similarity was also  
136 present for the individual cancer types (Pearson's  $r = 0.91$ ,  $P = 7.5 \times 10^{-8}$ ), with the strongest  
137 signals again observed for bladder cancer and metastatic melanoma (Fig. 2c). The fact that  
138 a set of randomly generated mutations, upon which selection cannot have acted, gave  
139 results that closely mimicked those from actual mutation data casts doubt on the apparent  
140 neoantigen depletion signals. As the simulated and real mutations were only matched with  
141 respect to trinucleotide substitution types, this analysis suggests that sequence differences  
142 between HLA-binding and non-binding regions, combined with specific sequence  
143 preferences of relevant mutagenic exposures, introduce biases in n/s ratios, leading to  
144 apparent signals of neoantigen depletion.

145 We noted that these findings were robust to the way HLA-binding capacity was  
146 determined. Determining HLA affinities using patient-specific HLA genotypes (rather than the  
147 six most frequent alleles), focusing on the best binding allele only and using a more stringent  
148  $K_d$  cut-off of 50 nM or a percentile-based cut-off of 1%, did not substantially alter the  
149 observed reduction in HBMR values (Supplementary Fig. 4). Similar results were also  
150 obtained when the analysis was restricted to genomic regions encoding known epitopes  
151 from IEDB (immune epitope database; Supplementary Fig. 5).

152 While the exclusion of non-expressed or cancer driver genes did not change the  
153 observed differences between tumor types either (Supplementary Fig. 4), we observed a  
154 lower overall percentage of somatic mutations in HLA-binding regions for expressed  
155 compared to non-expressed genes (21.7% vs. 28.3% respectively for the pan-cancer  
156 dataset, Fisher's exact test  $P = 0$ ), and an opposite effect for driver compared to non-driver  
157 genes (18.8% vs. 22.8% respectively,  $P = 7.6 \times 10^{-238}$ ; Supplementary Fig. 6). Similar  
158 differences were observed for both non-synonymous and synonymous mutations, again  
159 raising doubts about a putative interpretation as immunogenic selection signals. These  
160 findings also imply that mutations in non-expressed transcripts should not be used as

161 background reference when studying immunogenic selection pressures in cancer genomics  
162 data.

163 **Different trinucleotide substitution probabilities explain lower non-synonymous**  
164 **mutation rates in HLA-binding regions.**

165 To better understand the association between trinucleotide substitution types and HLA-  
166 binding regions, we simulated all possible point mutations in 17,992 genes (21,203,704  
167 synonymous and 67,766,542 non-synonymous mutations; Fig. 3a) and used the HBMR  
168 metric to quantify the difference between expected mutation rates in HLA-binding and non-  
169 binding regions for each trinucleotide substitution type. There was a notable variability  
170 between the trinucleotide substitution types, with HBMR values ranging from 0.35 for  
171 TCT>TGT substitutions to 2.07 for ATG>ACG substitutions (Fig. 3b). The trinucleotide  
172 substitution types with the lowest HBMR values were the most abundant in the cancer types  
173 with low overall HBMRs (e.g. 23.9% of all malignant melanoma mutations are TCC>TTC, the  
174 trinucleotide substitution type with the second to lowest HBMR; Supplementary Fig. 7).  
175 Remarkably, many of the substitution types with the lowest HBMR values were TCN>TNN  
176 (Fig. 3b), and a strong negative correlation was indeed observed between a cancer type's  
177 HBMR value and its proportion of TCN>TNN mutations (Pearson's  $r = -0.81$ ,  $P = 2.4 \times 10^{-5}$ ;  
178 Supplementary Fig. 7). Mutational signatures 2 and 3 (APOBEC-related) and the UV-  
179 induced signature 7, which are both related to these patterns, consequently had the lowest  
180 HBMR values (Supplementary Fig. 7).

181 **High synonymous mutation probabilities in hydrophobic amino acid codons correlate**  
182 **to lower perceived mutation rates in HLA-binding regions.**

183 We next aimed to explain the association between trinucleotide substitution types and HLA-  
184 binding properties. Because different sequence contexts imply different amino acid codon  
185 probabilities on the one hand, while different physicochemical properties of amino acids  
186 influence binding to HLA on the other hand, we investigated the relationships between



187 trinucleotide substitution types, the amino acid content of peptides, and their expected  
188 HMBR values.

189 We first focused on the correlation between HMBR values and amino acid classes  
190 (hydrophobic, polar or charged) in our annotated genome. For synonymous mutations, a  
191 strong negative correlation was observed between a trinucleotide substitution type's HMBR  
192 value and the frequency of hydrophobic amino acid codons (Spearman's  $r = -0.61$ ,  $P = 8.1 \times$   
193  $10^{-11}$ ; Fig. 3b), while an opposite, weaker and positive correlation was noted for non-  
194 synonymous mutations (Spearman's  $r = 0.30$ ,  $P = 4.2 \times 10^{-3}$ ; Fig. 3b). This effect was mainly  
195 related to Leu, Val and Iso (Supplementary Fig. 8); hydrophobic amino acids encoded by  
196 codons with a thymine on the second codon position (Supplementary Fig. 9). Combined with  
197 the observation that most of the corresponding trinucleotide substitution types conform to the  
198 pattern TCN>TNN, this association can be explained by the upstream T of the substitution  
199 type matching with the T at the second codon position and the substituted nucleotide  
200 matching with the third codon position (Fig. 3c). Indeed, when a codon with a T at the  
201 second position is hydrophobic, any mutation involving the third position of a Leu or Val  
202 codon always results in a synonymous mutation. This is also the case for most mutations  
203 that affect the same position in Ile and for some mutations at the Phe codon as exemplified  
204 in Figure 3c.

205 Secondly, as hydrophobic amino acids are known to influence HLA-binding  
206 affinities<sup>27</sup>, we determined the correlation between the number of amino acids from a certain  
207 class in a nonapeptide and its HLA-binding capacity. By randomly sampling from 1 million  
208 coding regions and determining the translated peptides' HLA-binding affinity, we observed a  
209 positive association between the number of hydrophobic amino acids in a peptide and its  
210 HLA-binding capacity (logistic regression coefficient  $\beta = 0.48$ , Fig. 3d and Supplementary  
211 Fig. 10).

212 These results demonstrate that certain trinucleotide substitution types, like  
213 TCN>TNN, which occur frequently in metastatic melanoma, bladder cancer and cervical  
214 cancer, are likely to lead to synonymous mutations in Leu, Val and Ile codons. Because

215 these amino acids are more frequent in HLA-binding peptides, this leads to lower perceived  
216 non-synonymous mutation rates when synonymous mutations are used as a background  
217 reference. The earlier described difference in apparent neoantigen depletion in expressed vs.  
218 non-expressed genes is also related to hydrophobic amino acid content, as a gene  
219 enrichment analysis of non-expressed genes showed a strong membrane protein  
220 enrichment (e.g. olfactory receptors; Supplementary Fig. 6).

221 **Weak to absent neoantigen depletion signals after correcting for trinucleotide**  
222 **substitution effects.**

223 Our study shows that differential mutation rates between HLA binding and non-binding  
224 peptides mainly result from differences in trinucleotide substitution probabilities. We next  
225 aimed to determine whether any remaining signal of neoantigen depletion would be  
226 detectable after correcting for these trinucleotide substitution effects.

227 As a first approach, we normalized the observed HBMR value to its expected value  
228 for each cancer, under a trinucleotide substitution model and considering the HLA-binding  
229 annotation developed in this study (see Methods). We reanalyzed all cancers and observed  
230 a disappearance of neoantigen depletion signals, except for a limited signal in lung cancer  
231 (Fig. 4a and Supplementary Table 2). In line with our earlier findings (Supplementary Fig. 4),  
232 results did not substantially change when different criteria were used to calculate HLA  
233 binding capacity or when mutations were called using the more recent MC3 mutation caller<sup>28</sup>  
234 (Supplementary Fig. 11). Similarly, dN/dS values did not suggest any signal of negative  
235 selection after correcting for differing trinucleotide sequence contexts in HLA binding vs.  
236 non-binding regions (Supplementary Fig. 12).

237 Notably, correcting using mutation probabilities derived from the SSB7 or other  
238 models that do not consider the complete adjacent sequence context resulted in corrected  
239 signals falsely suggestive of neoantigen depletion in e.g. melanoma and bladder cancer (Fig.  
240 4a and Supplementary Fig. 12). Conversely, normalization using an extended sequence

241 context (pentanucleotide substitution model) further decreased the apparent selection  
242 signals, with loss of significance in lung squamous cell carcinoma (Fig. 4a,b).

243 The previous results were all derived for a prototypical HLA genotype and for the  
244 reference genome (i.e. wild-type peptides). While this approach was useful in gathering new  
245 insights into associations between substitution types and HLA affinities, there is a risk of  
246 missing selection signals that are HLA genotype-specific and/or only act on mutations that  
247 result in new HLA binders (i.e. hit the HLA-binding residues of a nonapeptide, rather than the  
248 CTL contact residues). We thus searched for neoantigen depletion signals in mutated HLA-  
249 binding peptides, where binding affinities were predicted for sample-specific genotypes. We  
250 noted that only 1.88% of all non-synonymous mutations resulted in a non-binding peptide  
251 gaining HLA-binding properties (Supplementary Fig. 13). Similar numbers (1.92%) were  
252 found using our simulated mutation database, thus again providing no convincing support for  
253 selection acting on these specific mutations.

254 Finally, given that we have shown that synonymous mutation counts are particularly  
255 vulnerable to the effects of mutational signatures, we considered a selection metric  
256 ( $dN_{\text{HLA}}/dN_{\text{nonHLA}}$ ) that was independent of synonymous mutations. This metric compares the  
257 observed ratio between the number of non-synonymous mutations in HLA-binding and non-  
258 binding peptides with the corresponding expected ratio. The latter was determined for each  
259 HLA genotype from all TCGA samples, using mutated peptides from 960,000 randomly  
260 simulated mutations (10,000 for each trinucleotide substitution type) and considering the  
261 aggregated mutational signature from each cancer type (Fig. 5a,b). By normalizing the  
262 observed to the expected ratios for each sample, all tumor types were reanalyzed for  
263 putative selection signals. This analysis generally confirmed the absence of detectable  
264 neoantigen depletion, except for a signal in cervical cancer (median  $dN_{\text{HLA}}/dN_{\text{nonHLA}} = 0.91$ ,  
265 one-sample Wilcoxon signed-rank test  $P = 2.4 \times 10^{-4}$ ; Fig. 5c and Supplementary Table 2).  
266 Further,  $dN_{\text{HLA}}/dN_{\text{nonHLA}}$  did not correlate with immune cytolytic activity (Supplementary Fig.  
267 14). Notably, 3 out of 19 tumor types had values significantly above 1. These signals were  
268 comparable in effect size to cervical cancer, most pronounced in melanoma (median

269  $dN_{\text{HLA}}/dN_{\text{nonHLA}} = 1.08$ ,  $P = 1.2 \times 10^{-10}$ ), and remained when using a pentanucleotide rather  
270 than trinucleotide model (Supplementary Fig. 14). As these positive signals are unlikely to  
271 indicate true positive selection, they may rather reflect limitations of the  $dN_{\text{HLA}}/dN_{\text{nonHLA}}$  model,  
272 which does not consider synonymous mutation rates. Finally, neoantigen depletion signals  
273 were absent when the number of non-synonymous mutations in HLA-binding peptides was  
274 normalized to an expected number that was estimated directly from the pan-cancer dataset,  
275 as suggested previously<sup>10</sup> (Supplementary Fig. 14). Notably, we observed that the  
276 neoantigen depletion signals in colorectal and kidney cancer, as reported by Rooney et al.<sup>10</sup>,  
277 disappeared after excluding samples with miscalled HLA genotypes from the original dataset  
278 (results obtained using authors' source code; Supplementary Fig. 14).

279 Taken together, these results point to a general absence of detectable neoantigen  
280 depletion signals in large-scale mutation data from untreated tumors and emphasize the  
281 importance of using accurate background mutation models to correct for sequence biases  
282 introduced by relevant mutational processes.

## 283 **DISCUSSION**

284 In this study, we initially observed an apparent reduction of somatic point mutations in  
285 genomic regions encoding HLA-binding nonapeptides. Rather than being an effect of  
286 negative selection acting on immunogenic mutations, we demonstrated correlative  
287 relationships between the probability of mutagenesis in different nucleotide sequences and  
288 predicted HLA affinities for corresponding peptides. In particular, the number of hydrophobic  
289 amino acids are a major determinant of HLA binding capacity for a peptide while  
290 simultaneously being a strong determinant of mutation rate, depending on the mutational  
291 processes at play. When correcting for these correlations, detectable negative selection  
292 signals were weak to absent. Our results demonstrate that mutation rate differences  
293 between peptides with variable HLA affinities should be interpreted with care and have broad  
294 relevance for other studies that derive selection signals from HLA affinity predictions.

295 To detect immunogenic selection signals, we initially annotated the human exome  
296 with respect to HLA-binding capacity by determining which segments are translatable to  
297 HLA-binding peptides, for simplicity assuming a single prototypical HLA genotype for all  
298 samples. This implies a focus on wild-type peptides under the hypothesis that mutations in  
299 CTL contact residues are subject to negative selection pressures. Using this annotation, the  
300 approach can be easily reproduced on any mutation dataset, without the need for complex  
301 and time-consuming HLA-typing or HLA affinity predictions. The theoretical drawback is that  
302 this does not capture neoantigenic mutations that lead to new HLA-binding peptides (i.e.  
303 increase the HLA affinities) and/or effects that are HLA genotype-specific. However,  
304 additional analyses addressing patient-specific HLA genotypes as well as *de novo* HLA-  
305 binding peptides likewise failed to produce strong support for neoantigen depletion signals.

306 Synonymous mutations are often used as a background mutation reference when  
307 analyzing non-synonymous substitutions with respect to selection, resulting in metrics such  
308 as dN/dS. Recent studies have shown that these metrics get confounded when not  
309 considering the adjacent sequence context<sup>22,23</sup>. A key finding of our study is that simplistic  
310 substitution models will lead to biased immunogenic selection signals, due to HLA affinity  
311 predictions also being sequence dependent. An important advantage of any metric that  
312 considers synonymous mutations as a background reference (like HBMR) is that any  
313 unexpected property that equally effects synonymous and non-synonymous mutation rates  
314 will be cancelled out (such as differential mutation burdens in expressed and non-expressed  
315 genes). However, given that we observed strong dependencies specifically between  
316 synonymous mutation probabilities and HLA-binding properties of corresponding encoded  
317 peptides, leaving synonymous mutations out of the equation may also have advantages. We  
318 did this by considering the ratio between the observed number of non-synonymous  
319 mutations in HLA-binding and non-binding regions and normalizing this ratio to an expected  
320 ratio, estimated under a trinucleotide substitution model for each individual HLA genotype.  
321 Calculation of the resulting  $dN_{\text{HLA}}/dN_{\text{nonHLA}}$  metric for each sample did not provide clear  
322 evidence of neoantigen depletion, similar to our initial analysis taking synonymous mutations

323 into account. We could only detect a weak signal in cervical cancer and demonstrated that  
324 the previously reported neoantigen depletion signal in colorectal adenocarcinoma<sup>10</sup> was due  
325 to HLA genotyping problems in samples that were later removed from TCGA. Notably, the  
326  $dN_{HLA}/dN_{nonHLA}$  approach also indicated positive signals in some cancers, at effect sizes  
327 comparable to the depletion in cervical cancer. Since positive selection in HLA-binding  
328 regions is improbable, this likely reflects limitations in the accuracy of the expectation model,  
329 casting doubt on the observed negative signal in cervical cancer as well. While this may  
330 reflect exclusion of synonymous mutations in this metric, it can also be noted that mutational  
331 signatures were here determined at the tumor type level, and it is possible that consideration  
332 of patient-specific mutational signatures from whole genome sequencing datasets may  
333 potentiate more refined analyses in the future.

334 In addition to point mutations, which have been the main focus of studies of  
335 neoantigen depletion, future studies should also address frameshifting indels in this context.  
336 This is a different challenge, as single indels may generate large numbers of unnatural  
337 peptides through introduction of novel open reading frames, which may or may not be  
338 subject to nonsense-mediated decay<sup>29</sup>. Consistently, indels have been described as more  
339 strongly associated with response to immunotherapy<sup>30</sup>, and it can be noted that  
340 microsatellite unstable colon cancers, which harbor larger numbers of indels, appear  
341 responsive to checkpoint inhibitors while normal colon carcinomas are not<sup>31</sup>.

342 In summary, our results indicate that signals of neoantigen depletion, detected using  
343 HLA affinity predictions, are overall weak to absent in the untreated cancer genome. While  
344 we cannot exclude that this is related to poor accuracy to predict neoantigen formation  
345 (Supplementary Fig. 2), it is noteworthy that signals of negative selection in general are  
346 weak in cancer mutation data<sup>22,23,32,33</sup>. Therefore, either only a very small fraction of  
347 predicted neoantigenic sites are immunogenic, or the lack of negative selection signals  
348 suggests that developing tumors possess or evolve efficient immune evasion mechanisms  
349 (e.g. *HLA* loss or *PDL1* amplification). If this is indeed the case, detectable signals of

350 neoantigen depletion are only expected in the absence of these escape mechanisms, such  
351 as after ICB therapy<sup>21</sup>.

## 352 **ACKNOWLEDGEMENTS**

353 The results published here are in whole or part based upon data generated by TCGA.  
354 Information about TCGA and the investigators and institutions who constitute the TCGA  
355 research network can be found at <http://cancergenome.nih.gov>. We are most grateful to the  
356 patients, investigators, clinicians, technical personnel, and funding bodies who contributed to  
357 TCGA, thereby making this study possible.

358 This work was supported by grants from Wenner-Gren Foundation (SSv2017-005 to  
359 E.L.), the Swedish Cancer Society (CAN 2015/541 to E.L.), Knut and Alice Wallenberg  
360 Foundation (KAW 2014.0057 and KAW 2015.0144 to E.L.), Swedish Medical Research  
361 Council (2018-02852 to E.L.), Swedish Foundation for Strategic Research (RB13-0204 to  
362 E.L.), EMBO (STF7729 to J.V.d.E.) and Cancer Research UK (C14303/A17197 and A21141  
363 to M.L.M.).

## 364 **AUTHOR CONTRIBUTIONS**

365 J.V.d.E., E.L. and M.L.M. designed and conceptualized the study. A.J.-S. provided input on  
366 study design and contributed to the interpretation of the results. J.V.d.E. was responsible for  
367 data analysis and drafted the manuscript. All authors discussed the results, edited and  
368 finalized the manuscript.

## 369 **COMPETING INTERESTS STATEMENT**

370 The authors declare they have no conflicts of interest.

371

372 **REFERENCES**

- 373 1. Vogelstein, B. *et al.* Cancer genome landscapes. *Science* **339**, 1546–1558 (2013).
- 374 2. Cancer Genome Atlas Research, N. *et al.* The Cancer Genome Atlas Pan-Cancer  
375 analysis project. *Nat. Genet.* **45**, 1113–1120 (2013).
- 376 3. Alexandrov, L. B. *et al.* Signatures of mutational processes in human cancer. *Nature*  
377 **500**, 415–421 (2013).
- 378 4. Hanahan, D. & Weinberg, R. A. Hallmarks of cancer: The next generation. *Cell* **144**,  
379 646–674 (2011).
- 380 5. Dunn, G. P., Old, L. J. & Schreiber, R. D. The three Es of cancer immunoediting.  
381 *Annu. Rev. Immunol.* **22**, 329–360 (2004).
- 382 6. DuPage, M., Mazumdar, C., Schmidt, L. M., Cheung, A. F. & Jacks, T. Expression of  
383 tumour-specific antigens underlies cancer immunoediting. *Nature* **482**, 405–409  
384 (2012).
- 385 7. Pardoll, D. M. The blockade of immune checkpoints in cancer immunotherapy. *Nat.*  
386 *Rev. Cancer* **12**, 252–264 (2012).
- 387 8. Hodi, F. S. *et al.* Improved survival with ipilimumab in patients with metastatic  
388 melanoma. *N. Engl. J. Med.* **363**, 711–723 (2010).
- 389 9. Sharma, P. & Allison, J. P. Immune checkpoint targeting in cancer therapy: toward  
390 combination strategies with curative potential. *Cell* **161**, 205–214 (2015).
- 391 10. Rooney, M. S., Shukla, S. A., Wu, C. J., Getz, G. & Hacohen, N. Molecular and  
392 genetic properties of tumors associated with local immune cytolytic activity. *Cell* **160**,  
393 48–61 (2015).
- 394 11. Shukla, S. A. *et al.* Comprehensive analysis of cancer-associated somatic mutations  
395 in class I HLA genes. *Nat. Biotechnol.* **33**, 1152–1158 (2015).
- 396 12. McGranahan, N. *et al.* Allele-specific HLA loss and immune escape in lung cancer  
397 evolution. *Cell* **171**, 1259–1271.e11 (2017).



- 398 13. Davoli, T., Uno, H., Wooten, E. C. & Elledge, S. J. Tumor aneuploidy correlates with  
399 markers of immune evasion and with reduced response to immunotherapy. *Science*  
400 **355**, eaaf8399 (2017).
- 401 14. Rutledge, W. C. *et al.* Tumor-infiltrating lymphocytes in glioblastoma are associated  
402 with specific genomic alterations and related to transcriptional class. *Clin. Cancer Res.*  
403 **19**, 4951–4960 (2013).
- 404 15. Brown, S. D. *et al.* Neo-antigens predicted by tumor genome meta-analysis correlate  
405 with increased patient survival. *Genome Res.* **24**, 743–750 (2014).
- 406 16. Rosenthal, R. *et al.* Neoantigen-directed immune escape in lung cancer evolution.  
407 *Nature* **567**, 479–485 (2019).
- 408 17. Van Allen, E. M. *et al.* Genomic correlates of response to CTLA-4 blockade in  
409 metastatic melanoma. *Science* **350**, 207–211 (2015).
- 410 18. Snyder, A. *et al.* Genetic basis for clinical response to CTLA-4 blockade in melanoma.  
411 *N. Engl. J. Med.* **371**, 2189–2199 (2014).
- 412 19. Rizvi, N. A. *et al.* Cancer immunology. Mutational landscape determines sensitivity to  
413 PD-1 blockade in non-small cell lung cancer. *Science* **348**, 124–128 (2015).
- 414 20. Zapata, L. *et al.* Negative selection in tumor genome evolution acts on essential  
415 cellular functions and the immunopeptidome. *Genome Biol.* **19**, 67 (2018).
- 416 21. Riaz, N. *et al.* Tumor and microenvironment evolution during immunotherapy with  
417 nivolumab. *Cell* **171**, 934-949.e15 (2017).
- 418 22. Van den Eynden, J. & Larsson, E. Mutational signatures are critical for proper  
419 estimation of purifying selection pressures in cancer somatic mutation data when  
420 using the dN/dS metric. *Front. Genet.* **8**, 74 (2017).
- 421 23. Martincorena, I. *et al.* Universal patterns of selection in cancer and somatic tissues.  
422 *Cell* **171**, 1029-1041.e21 (2017).
- 423 24. Lawrence, M. S. *et al.* Mutational heterogeneity in cancer and the search for new  
424 cancer-associated genes. *Nature* **499**, 214–218 (2013).
- 425 25. Marty, R. *et al.* MHC-I genotype restricts the oncogenic mutational landscape. *Cell* **17**,

- 426 1272–1283.e15 (2017).
- 427 26. Paul, S. *et al.* HLA class I alleles are associated with peptide-binding repertoires of  
428 different size, affinity, and immunogenicity. *J. Immunol.* **191**, 5831–5839 (2013).
- 429 27. Chowell, D. *et al.* TCR contact residue hydrophobicity is a hallmark of immunogenic  
430 CD8+ T cell epitopes. *Proc. Natl. Acad. Sci. USA* **112**, E1754-E1762 (2015).
- 431 28. Ellrott, K. *et al.* Scalable open science approach for mutation calling of tumor exomes  
432 using multiple genomic pipelines. *Cell Syst.* **6**, 271-281.e7 (2018).
- 433 29. Turajlic, S. *et al.* Insertion-and-deletion-derived tumour-specific neoantigens and the  
434 immunogenic phenotype: a pan-cancer analysis. *Lancet Oncol.* **18**, 1009–1021 (2017).
- 435 30. Mandal, R. *et al.* Genetic diversity of tumors with mismatch repair deficiency  
436 influences anti-PD-1 immunotherapy response. *Science* **364**, 485–491 (2019).
- 437 31. Stein, A. & Folprecht, G. Immunotherapy of colon cancer. *Oncol. Res. Treat.* **41**, 282–  
438 285 (2018).
- 439 32. Van den Eynden, J., Basu, S. & Larsson, E. Somatic mutation patterns in hemizygous  
440 genomic regions unveil purifying selection during tumor evolution. *PLoS Genet.* **12**,  
441 e1006506 (2016).
- 442 33. Weghorn, D. & Sunyaev, S. Bayesian inference of negative and positive selection in  
443 human cancers. *Nat. Genet.* **49**, 1785–1788 (2017).

444

445

446 **FIGURE LEGENDS**

447 **Figure 1 | Development of an HLA-binding genomic annotation to detect somatic**  
448 **mutations under immunogenic selective pressure.**

449 **a**, Neoantigen formation is expected when a non-synonymous mutation leads to a structural  
450 change in the CTL (CD8+ cytotoxic T lymphocyte) contact residues of an HLA-binding  
451 nonapeptide. This can result in CTL-mediated apoptotic cell death and hence negative  
452 selection of the underlying somatic mutation. TCR, T cell receptor; MHC-I, type I major  
453 histocompatibility complex. **b**, Binding affinities of all possible nonapeptides were determined  
454 for the six most common HLA alleles as indicated. Peptides were considered HLA-binding  
455 when their aggregated  $K_d$  over the six alleles was below 500 nM (see Methods); HLA-  
456 binding peptides mapped to 22.1% of the exome as indicated.

457 **Figure 2 | Analysis of somatic mutation rates in HLA-binding annotated genomic**  
458 **regions.**

459 **a**, Contingency table showing the total number of synonymous (s) and non-synonymous (n)  
460 mutations in the HLA-binding and non-binding exome. The HLA-binding mutation ratio  
461 (HBMR) indicates the ratio of n/s in HLA-binding to non-binding regions. **b**, Bar plot  
462 comparing the n/s ratios of observed and simulated mutations. **c**, HBMR calculated for  
463 observed and simulated mutations from 19 cancer types containing at least 10,000 somatic  
464 mutations per cancer type. Error bars indicate 95% confidence intervals, calculated using  
465 two-sided Fisher's exact test. Pearson correlation coefficient ( $r$ ) and  $P$  value indicated on top  
466 left. See Supplementary Table 1 for cancer type abbreviations and sample sizes.

467 **Figure 3 | Association between trinucleotide substitution types and HLA-binding**  
468 **properties.**

469 **a**, All possible synonymous and non-synonymous mutations were determined in 17,992  
470 genes. Pie charts indicate the proportions of mutations that are located in HLA-binding  
471 regions. **b**, Bar plot on top indicates the expected HBMR value for each trinucleotide

472 substitution type, determined from all possible mutations from a given type in the complete  
473 exome (numbers shown in **a**). Main substitution types are colored as indicated by the legend  
474 on top left. Note that HBMR values are not derivable for four trinucleotide substitution types  
475 (ATT>AAT, ATT>AGT, ACT>AGT and ACT>AAT) due to the absence of synonymous  
476 mutations resulting from these substitution types (e.g. an ATT>AAT substitution can never  
477 be synonymous). TCN>TNN substitutions are indicated by red asterisks. Below the bar plot,  
478 the frequency of synonymous and non-synonymous mutations hitting hydrophobic amino  
479 acids is indicated for each substitution type (scale indicated on bottom right). Loess  
480 regression line in red with Spearman correlation coefficient ( $r$ ) and  $P$  value indicated on top  
481 right (correlation between HBMR and mutation frequency for 92 different substitution types).  
482 **c**, Illustration of TCN>TNN mutations mainly resulting in synonymous mutations in  
483 hydrophobic amino acid codons. **d**, Logistic regression line indicating the correlation  
484 between a nonapeptide's mean number of hydrophobic/charged/polar amino acids (0 to 9)  
485 and the HLA-binding probability. Regression coefficients ( $\beta$ ) are given for each amino acid  
486 class. The mean number of amino acids for each class was determined for 1 million random  
487 exome locations (9 nonapeptides per position) to make the analysis comparable to the other  
488 analyses. A similar analysis on individual nonapeptides is shown in Supplementary Figure  
489 10.

490 **Figure 4 | Weak to absent neoantigen depletion signals after correcting for**  
491 **trinucleotide-based mutational signature effects.**

492 **a**, Bar plot showing normalized HBMR values for 19 different cancer types. HBMR values  
493 were obtained by normalization of the observed HBMR values to the expected tumor-type  
494 specific values. The latter were calculated using mutation probabilities derived from different  
495 models as indicated on top left. Error bars indicate 95% confidence intervals, calculated  
496 using two-sided Fisher's exact test. See Supplementary Table 1 for cancer type  
497 abbreviations and sample sizes and Supplementary Table 2 for detailed results. **b**,  
498 Comparison of HBMR deviations from 1 after normalization using different substitution

499 models as indicated. Each dot represents a cancer type. Median values are indicated by  
500 horizontal lines.

501 **Figure 5 | An HLA genotype-specific analyses of mutated peptides confirms the**  
502 **absence of neoantigen depletion signals in most tumor types.**

503 **a**, Methodological approach. For each trinucleotide substitution type (i), 10,000 mutations  
504 were randomly simulated (960,000 mutations in total). The expected number of non-  
505 synonymous mutations in HLA-binding and non-binding peptides were derived for each  
506 substitution type considering the mutated peptides' HLA affinities for the sample-specific  
507 HLA genotype (heatmap on bottom). From these numbers, the expected ratio between non-  
508 synonymous mutations in HLA-binding and non-binding peptides was calculated using the  
509 substitution probabilities of the corresponding cancer type (legoplot on top). **b**, Scatter plot  
510 shows the correlation between observed and expected ratios, with Pearson correlation  
511 coefficients ( $r$ ) and  $P$  values indicated on top left. **c**,  $dN_{\text{HLA}}/dN_{\text{nonHLA}}$  values were calculated  
512 for each TCGA sample and grouped by tumor types. Boxplots indicate median values and  
513 lower/upper quartiles with whiskers extending to 1.5x the interquartile range. Two-sided  
514 Wilcoxon signed-rank test was used to test deviation from 1.  $P$  values are given for cancers  
515 with  $q$  values below 0.1. Mutations in cancer driver genes or non-expressed genes were  
516 excluded. See Supplementary Table 1 for cancer type abbreviations and sample sizes and  
517 Supplementary Table 2 for detailed results.

518 **METHODS**

519 **TCGA mutation and expression data.**

520 MuTect2-called whole exome sequencing (WES) mutation annotation format (maf) files from  
521 all 33 available cancer types from The Cancer Genome Atlas (TCGA) were downloaded  
522 from the Genomic Data Commons (GDC) Data Portal (data release v7). Colon and rectal  
523 adenocarcinoma were considered as a single cancer type for the analysis. All mutation data  
524 were fused in a single mutation database and were converted from hg38 to hg19 using

525 UCSC's liftOver<sup>34</sup>. Variants were reannotated using ANNOVAR<sup>35</sup>. For each mutation, the  
526 main substitution type (i.e. C>A, C>G, C>T, T>A, T>C and T>G) was derived by converting  
527 each purine substitution to its complementary base substitution. To determine the  
528 trinucleotide substitution type, additional information was added regarding the identity of the  
529 upstream and downstream base. Sequence information was derived from UCSC hg19<sup>34</sup>.

530 TCGA Level 3 RNASeqV2 (RSEM normalized) mRNA expression data were  
531 downloaded from the Broad Institute TCGA Genome Data Analysis Center (2016): Firehose  
532 stddata\_\_2016\_01\_28 run (Broad Institute of MIT and Harvard; doi:10.7908/C11G0KM9).  
533 Expression data were fused in a single gene x sample matrix. Each mutation's gene  
534 expression value was added to the mutation database.

#### 535 **HLA typing.**

536 HLA typing of all TCGA samples was performed using Polysolver<sup>11</sup>. WES normal bam files  
537 from all available TCGA samples were accessed using FireCloud<sup>36</sup>, the HLA regions from  
538 the main HLA-alleles (HLA-A, HLA-B and HLA-C) in chromosome 6 (coordinates  
539 6:29909037-29913661; 6:31321649-31324964; 6:31236526-31239869) were extracted and  
540 the resulting bam files were downloaded. Polysolver was run on these bam files using  
541 default settings and without setting prior population probabilities, resulting in the successful  
542 genotyping of 8,968 TCGA samples. The resulting output was converted in a sample x HLA  
543 allele matrix. To validate this HLA typing, the derived frequencies for each HLA allele were  
544 compared with the allele frequencies from a healthy US blood donor population, downloaded  
545 from Allele frequency net<sup>37</sup> (Supplementary Fig. 1).

#### 546 **HLA affinity predictions and annotation of the HLA-binding genome.**

547 Using the R *GenomicRanges* package<sup>38</sup> and UCSC hg19 genome sequence information, a  
548 *GPos* object was created containing information about the complete exome. For each coding  
549 DNA sequence (CDS) position, the amino acid sequences of the nine possible translated 9-  
550 mers (nonapeptides) were determined using Ensembl 75. Genes with unavailable or

551 ambiguous protein information in Ensembl were discarded, resulting in a *GPos* object  
552 containing nonapeptide information of 17,992 genes. HLA affinities of these nonapeptides  
553 were predicted for the most frequent HLA alleles (A02:01, A01:01, B07:02, B08:01, C07:01,  
554 C07:02; a combination referred to as the prototypical genotype) using netMHCpan3.0<sup>39</sup>. For  
555 each CDS position, the best binding peptide (peptide with the lowest predicted  $K_d$  value) was  
556 determined for each of the six HLA alleles. Finally, one aggregated  $K_d$  value was calculated  
557 using the harmonic mean value of the  $K_d$  values of the six different peptides (one from each  
558 allele) and all genomic regions with aggregated  $K_d$  values below 500 nM were considered as  
559 HLA-binding regions. The same methodology was used to predict HLA affinities in TCGA  
560 somatic mutation data. These TCGA predictions were done for both the prototypical and the  
561 sample-specific HLA genotype (specific combination of two HLA-A, two HLA-B and two HLA-  
562 C alleles) and for wild-type as well as mutated peptides.

### 563 **Simulation of somatic mutations.**

564 All possible point mutations were determined for 17,992 genes by considering for each CDS  
565 position the three possible substitutions (any nucleotide can be substituted in three different  
566 nucleotides). ANNOVAR<sup>35</sup> was used to annotate the variants and determine the reference  
567 and alternative amino acids for each mutation. This information was added to the higher  
568 described *GPos* object.

569 To determine the expected somatic mutation rates in the absence of any selection  
570 pressure, a simulated mutation database was created, with a similar size as the TCGA  
571 mutation database. To match this simulation database for differences in trinucleotide  
572 substitution probabilities, we randomly sampled the observed number of mutations from  
573 each corresponding substitution type from the *GPos* object. Like for the observed TCGA  
574 mutations, HLA affinities were predicted for the wild-type and the mutated nonapeptides and  
575 for both the prototypical and the sample-specific genotype. The later was determined by  
576 scrambling the columns from the sample x HLA allele matrix. This way, completely random

577 HLA genotypes were generated, with the same allele frequency and mutation frequency per  
578 type as in the real data.

### 579 **Amino acid analysis.**

580 To derive the probability of any substitution type to hit a certain amino acid or class of amino  
581 acids, we used the *GPos* object containing all possible mutations and determined the amino  
582 acid frequency for each substitution type and separately for synonymous and non-  
583 synonymous mutations. Amino acids were grouped in three classes: hydrophobic (Gly, Ala,  
584 Pro, Val, Leu, Iso, Met, Trp and Phe), polar (Ser, Thr, Tyr, Asn, Gln and Cys) and charged  
585 (Lys, Arg, His, Asp and Glu).

### 586 **Calculation of the HLA-binding mutation ratio (HBMR) and related metrics.**

587 To quantify putative signals of immunogenic selection, we defined an HLA-binding mutation  
588 ratio (HBMR):

$$589 \quad HBMR = \frac{n_+/s_+}{n_-/s_-}$$

590 where  $n_+$  and  $n_-$  are the total number of non-synonymous mutations located in HLA-binding  
591 and non-binding regions, respectively. Similarly,  $s_+$  and  $s_-$  are the number of synonymous  
592 mutations in- and outside HLA-binding genomic regions. A similar metric, called the epitope  
593 mutation ratio (EMR) was calculated for the analysis of the IEDB epitopes. Here, + and –  
594 refer to the location inside and outside of epitope mapped regions. HBMR  $P$  values and 95%  
595 confidence intervals were calculated using a two-sided Fisher's exact test.

596  $dN/dS$  was calculated considering differences in specific trinucleotide substitution  
597 probabilities between cancer types<sup>22</sup>:

$$598 \quad \frac{dN}{dS} = \frac{n/\sum_i N_i P_i}{s/\sum_i S_i P_i}$$

with  $i \in \{A[C > A]A, \dots, T[T > G]T\}$  (96 substitution types)

599



600 where  $N_i$  and  $S_i$  are the number of (non-)synonymous sites with class  $i$  substitutions and  $P_i$  is  
 601 the probability of substitution class  $i$ .

602 The normalized HBMR was calculated as follows:

603 
$$\text{Normalized HBMR} = \frac{HBMR_{obs}}{HBMR_{exp}}$$

604 
$$\text{with } HBMR_{exp} = \frac{N_+/S_+}{N_-/S_-} = \frac{\sum_i N_{i+} P_i / \sum_i S_{i+} P_i}{\sum_i N_{i-} P_i / \sum_i S_{i-} P_i}$$

605 where  $N_{i+}$  and  $S_{i+}$  are the number of (non-)synonymous sites with class  $i$  substitutions in  
 606 HLA-binding regions,  $N_{i-}$  and  $S_{i-}$  are the number of (non-)synonymous sites with class  $i$   
 607 substitutions in non-HLA-binding regions respectively and  $P_i$  is the probability of substitution  
 608 class  $i$ .

609 The  $dN_{HLA}/dN_{nonHLA}$  ratio was calculated for each TCGA sample as follows:

610 
$$\frac{dN_{HLA}}{dN_{nonHLA}} = \frac{n_+/n_-}{N_+/N_-} = \frac{n_+/n_-}{\sum_i N_{i+} P_i / \sum_i N_{i-} P_i}$$

611 with variables as defined above, but with HLA affinities determined for mutated peptides  
 612 from individual genotypes. The number of HLA-binding and non-binding sites was  
 613 determined for each individual TCGA genotype, under a trinucleotide substitution model. To  
 614 achieve this, 960,000 substitutions were randomly sampled from the complete exome  
 615 (10,000 for each substitution type) and HLA affinities were predicted for all the mutations,  
 616 considering the cancer-type-specific mutational signature.

617 The ratio  $R$  of observed to expected neoantigens as described by Rooney *et al.*<sup>10</sup>  
 618 was calculated for each TCGA sample as follows:

619 
$$R = \frac{n_+/n}{N_+/N} = \frac{n_+/n}{\sum_i S_i \frac{\bar{N}_i \bar{N}_{i+}}{S_i \bar{N}_i} / \sum_i S_i \frac{\bar{N}_i}{S_i}}$$

620 where  $\bar{N}_i/S_i$  is the expected number of non-synonymous mutations per synonymous site and  
621  $\bar{N}_{i+}/\bar{N}_i$  refers to the expected number of HLA-binders per non-synonymous site, both for  
622 substitution type  $i$  and estimated empirically from the pan-cancer dataset. Note that these  
623 variables are similar to the originally defined variables  $\bar{N}_{s(m)}$  and  $\bar{B}_{s(m)}$ , respectively.  
624 Similarly,  $n_+$  and  $N_+$  were originally called  $B_{obs}$  and  $B_{pred}$ , while  $n$  and  $N$  were originally  
625 referred to as  $N_{obs}$  and  $N_{pred}$ . They were defined here as such to be consistent with the rest  
626 of the methodology.

627 Calculation of these metrics was always based on a trinucleotide substitution model  
628 as indicated ( $i$  index). The normalized HBMR,  $dN/dS$  and  $dN_{HLA}/dN_{nonHLA}$  were also  
629 calculated using alternative substitution models, either based on the six main substitution  
630 classes, pentanucleotide substitution classes or using the SSB7 model. The latter is based  
631 on the six main substitution classes but considers CpG mutations as a separate class<sup>20</sup>.

### 632 **Neoantigen depletion simulation and power analysis.**

633 All metrics developed in this study were evaluated using an *in silico* analysis of neoantigen  
634 depletion by removing increasing amounts of non-synonymous mutations hitting HLA-  
635 binding regions from the mutation dataset.

636 Statistical power of the HBMR metric was evaluated using the R *exact2x2* package  
637 (Fisher's exact test at significance level 0.05) for different amounts of neoantigen depletion,  
638 numbers of mutations and neoantigen prediction accuracies. For this analysis, the non-  
639 synonymous mutation proportion (71%) and HLA-binding proportion (22.1%) were fixed to  
640 values derived from the pan-cancer dataset and the HLA-binding annotation respectively.

641 For the power analysis of the  $dN_{HLA}/dN_{nonHLA}$  ratio, the ratios obtained from the  
642 simulated mutation database (containing no selection signals) were log-transformed to  
643 obtain a normal distribution. After resampling 1,000 times a predefined amount of values  
644 from this normal distribution and adding an *in silico* amount of neoantigen depletion, power  
645 was determined based on the number of significant deviations from 0 (corresponding to 1 in

646 non-logtransformed data) using Wilcoxon signed-rank test at  $P < 0.05$ . This analysis was  
647 performed again for different amounts of neoantigen depletion, sample numbers and  
648 neoantigen prediction accuracies.

#### 649 **Human epitope mapping.**

650 Data from 66,698 known human IEDB (Immune Epitope Database) epitopes were  
651 downloaded from synapse at <https://www.synapse.org/> (id syn11935058)<sup>20</sup>. These epitopes  
652 were mapped to the human genome (hg19) using the *proteinToGenome* function from the  
653 *ensemldb* R package and the *EnsDb.Hsapiens.v75* R library. Mapping was successful for  
654 66,536 (99.8%) epitopes.

#### 655 **Statistical analysis.**

656 The R statistical package was used for all data processing and statistical analysis. Details on  
657 statistical tests used are reported in the respective sections. Further information on research  
658 design is available in the Life Sciences Reporting Summary.

#### 659 **DATA AVAILABILITY**

660 This study is based on public data (open or controlled access) from The Cancer Genome  
661 Atlas Network. Downstream data and source code are available at zenodo  
662 (<https://doi.org/10.5281/zenodo.2621365> and <https://doi.org/10.5281/zenodo.3461642>,  
663 respectively).

#### 664 **METHODS-ONLY REFERENCES**

- 665 34. Rosenbloom, K. R. *et al.* The UCSC Genome Browser database: 2015 update.  
666 *Nucleic Acids Res.* **43**, D670-D681 (2014).
- 667 35. Wang, K., Li, M. & Hakonarson, H. ANNOVAR: functional annotation of genetic  
668 variants from high-throughput sequencing data. *Nucleic Acids Res* **38**, e164 (2010).
- 669 36. Birger, C. *et al.* FireCloud, a scalable cloud-based platform for collaborative genome

- 670 analysis: Strategies for reducing and controlling costs. *bioRxiv* 209494 (2017).  
671 doi:10.1101/209494
- 672 37. González-Galarza, F. F. *et al.* Allele frequency net 2015 update: new features for HLA  
673 epitopes, KIR and disease and HLA adverse drug reaction associations. *Nucleic*  
674 *Acids Res.* **43**, D784–D788 (2015).
- 675 38. Lawrence, M. *et al.* Software for computing and annotating genomic ranges. *PLoS*  
676 *Comput. Biol.* **9**, e1003118 (2013).
- 677 39. Nielsen, M. & Andreatta, M. NetMHCpan-3.0; improved prediction of binding to MHC  
678 class I molecules integrating information from multiple receptor and peptide length  
679 datasets. *Genome Med.* **8**, 33 (2016).

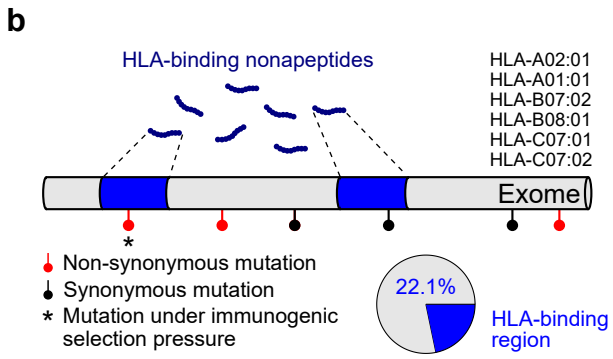
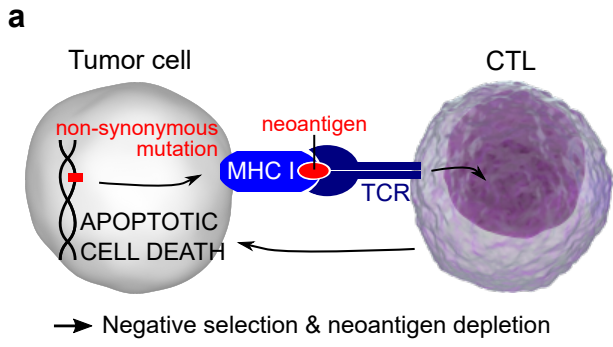


Figure 1

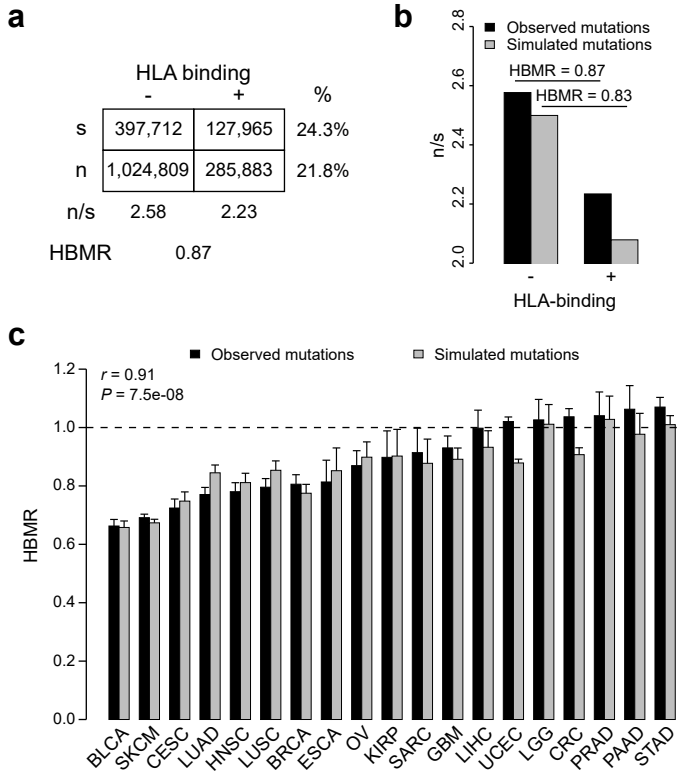


Figure 2



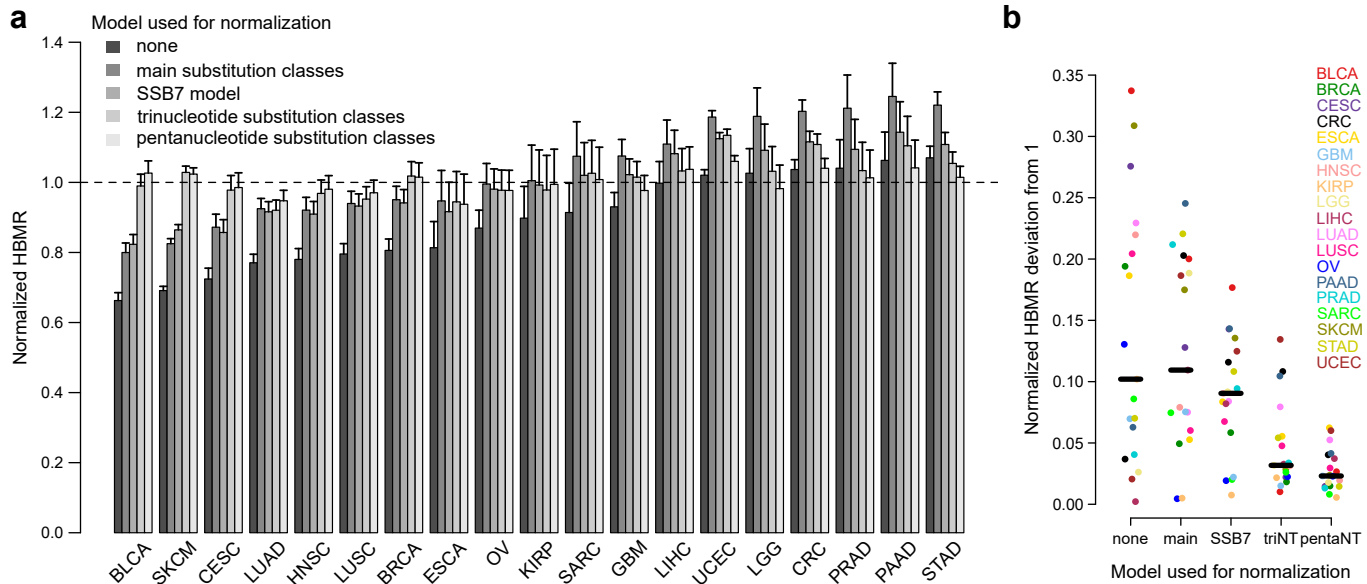


Figure 4



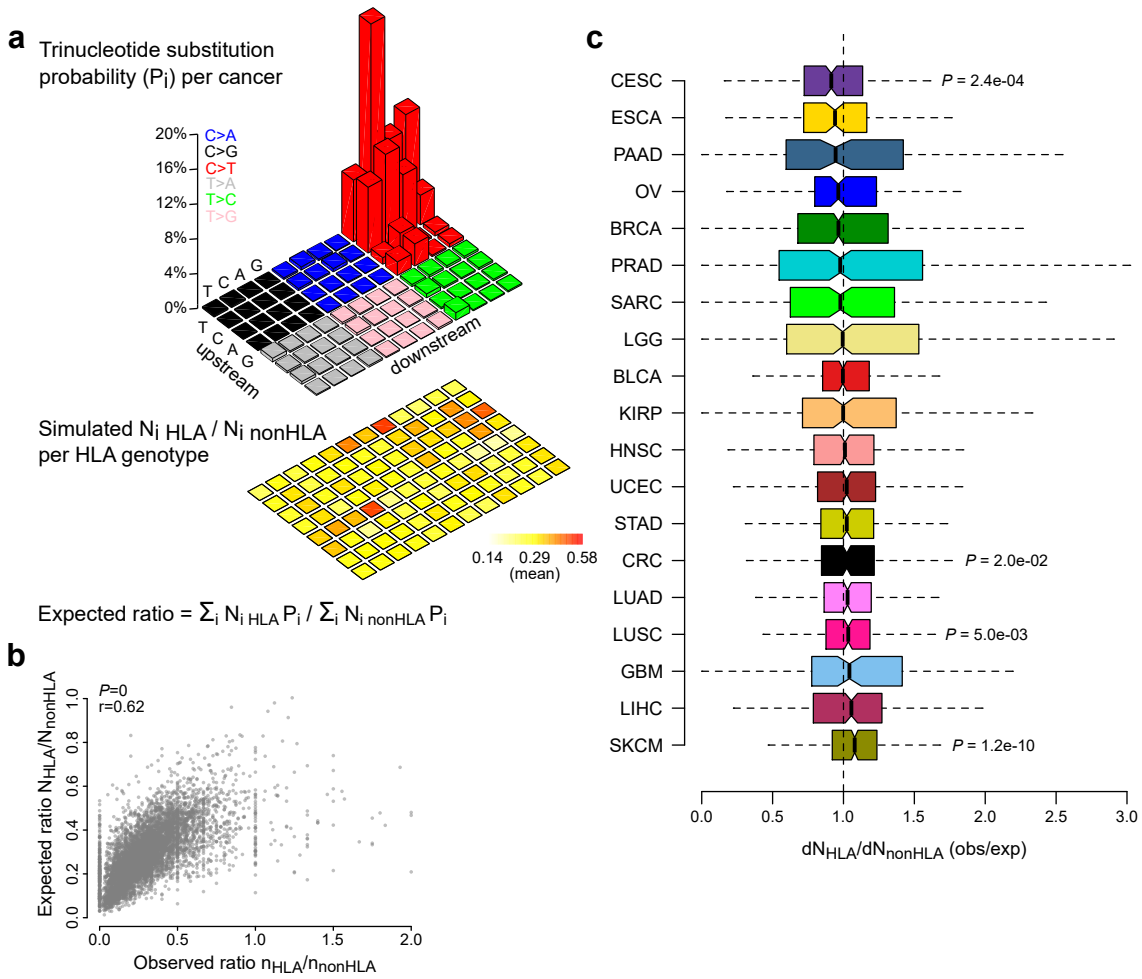


Figure 5